

Emergence of spatial curvature

Krzysztof Bolejko^{*1}

¹Sydney Institute for Astronomy, School of Physics, A28, The University of Sydney, NSW, 2006, Australia

March 3, 2022

Abstract

This paper investigates the phenomenon of emergence of spatial curvature. This phenomenon is absent in the Standard Cosmological Model, which has a flat and fixed spatial curvature (small perturbations are considered in the Standard Cosmological Model but their global average vanishes, leading to spatial flatness at all times). This paper shows that with the nonlinear growth of cosmic structures the global average deviates from zero. The analysis is based on the *silent universes* (a wide class of inhomogeneous cosmological solutions of the Einstein equations). The initial conditions are set in the early universe as perturbations around the Λ CDM model with $\Omega_m = 0.31$, $\Omega_\Lambda = 0.69$, and $H_0 = 67.8$ km s⁻¹ Mpc⁻¹. As the growth of structures becomes nonlinear, the model deviates from the Λ CDM model, and at the present instant if averaged over a domain \mathcal{D} with volume $V = (2150 \text{ Mpc})^3$ (at these scales the cosmic variance is negligibly small) gives: $\Omega_m^{\mathcal{D}} = 0.22$, $\Omega_\Lambda^{\mathcal{D}} = 0.61$, $\Omega_{\mathcal{R}}^{\mathcal{D}} = 0.15$ (in the FLRW limit $\Omega_{\mathcal{R}}^{\mathcal{D}} \rightarrow \Omega_k$), and $\langle H \rangle_{\mathcal{D}} = 72.2$ km s⁻¹ Mpc⁻¹. Given the fact that low-redshift observations favor higher values of the Hubble constant and lower values of matter density, compared to the CMB constraints, the emergence of the spatial curvature in the low-redshift universe could be a possible solution to these discrepancies.

1 Introduction

Astronomical constraints on the spatial curvature are often derived, not by a direct measurement, but by fitting a spatially homogeneous and isotropic model, or a linearly perturbed FLRW model, to observational data. The tightest constraints come from the early universe: the CMB data (TT+LowP+lensing) constrain the curvature at a percent level. If accompanied with the BAO data then the spatial flatness is confirmed with a sub-percent precision

*krzysztof.bolejko@sydney.edu.au

(Planck Collaboration et al., 2016). These constraints fit nicely with inflationary scenarios that predict spatial flatness of the early universe (Guth, 1981).

However, the spatial curvature of the FLRW models is very rigid, so fitting these models to the data is not equivalent to direct measurements, which do not provide such tight constraints (Räsänen et al., 2015). Investigations of nonlinear dynamics by Buchert & Carfora (2008) and also Roy et al. (2011) suggest that the overall spatial curvature of our universe may in fact be negative. Recently, using a Styrofoam model that consisted of the Szekeres cells, it was shown how the spatial curvature emerges due to the evolution of the cosmic structures (Bolejko, 2017b). This paper investigates this phenomenon further using a more general class of *silent universes*. The investigation is based on the Monte Carlo simulation that consist of 2×10^6 worldlines. These worldlines are evolved from the early universe to the present instant. Each worldline is characterized by density, expansion rate, shear, and Weyl curvature. From these quantities, the spatial curvature is evaluated, and it is shown that the global average evolves from zero and reaches non-negligible, negative values at the present instant. The structure of this paper is as follows: Sec. 2 briefly presents the *silent universes*; Sec. 3 presents the results of the Monte Carlo simulation and shows how the spatial curvature emerges due to nonlinear evolution (in the linear regime negative curvature of voids is compensated by positive curvature of overdense regions and so the global spatial curvature is zero); Sec 4 discusses the obtain results and speculates on possibility of detecting this phenomenon.

2 Silent Cosmology

The evolution of a relativistic system is set by its content (T_{ab}) and the space-time geometry ($G_{ab} - \Lambda g_{ab}$). In the 3+1 split, the system can be reduced to scalars (density, expansion rate), vectors (particle acceleration, rotation, particle flux, energy transfer, entropy flux), and tensors (shear, anisotropic stress-tensor, magnetic and electric parts of the Weyl curvature). On scales, above 2-5 Mpc (cf. matter horizon defined by Ellis & Stoeger (2009)) contribution from particle flux, pressure and viscosity, and rotation can be neglected, and the solution of the Einstein equations reduces to the *silent universe*, where each worldline evolves independently (hence ‘silent’), and the whole system is described by 4 scalars: density ρ , expansion Θ , shear Σ , and the Weyl curvature \mathcal{W} (Bruni et al., 1995; van Elst et al., 1997)

$$\dot{\rho} = -\rho\Theta, \quad (1)$$

$$\dot{\Theta} = -\frac{1}{3}\Theta^2 - \frac{1}{2}\kappa\rho - 6\Sigma^2 + \Lambda, \quad (2)$$

$$\dot{\Sigma} = -\frac{2}{3}\Theta\Sigma + \Sigma^2 - \mathcal{W}, \quad (3)$$

$$\dot{\mathcal{W}} = -\Theta\mathcal{W} - \frac{1}{2}\kappa\rho\Sigma - 3\Sigma\mathcal{W}, \quad (4)$$

where $\kappa = 8\pi G/c^4$. The change of (spatial) volume V is

$$\dot{V} = V\Theta, \quad (5)$$

and the spatial curvature \mathcal{R} follows from the ‘‘Hamiltonian’’ constraint

$$\frac{1}{6}\mathcal{R} = \frac{1}{3}\kappa\rho + \Sigma^2 - \frac{1}{9}\Theta^2 + \frac{1}{3}\Lambda. \quad (6)$$

Spatially homogeneous and isotropic FLRW models form a small subset of solutions of the above equations, with

$$\Sigma \equiv 0, \quad \mathcal{W} \equiv 0, \quad \Theta \equiv 3\frac{\dot{a}}{a}, \quad \mathcal{R} \equiv 6\frac{k}{a^2}, \quad (7)$$

where k is a constant, and $a(t)$ is a function of time. Using the equation for $\dot{\Theta}$ and the ‘‘Hamiltonian’’ constraint the evolutionary equations can be written in a more familiar form of the Friedmann equations

$$3\frac{\ddot{a}}{a} = -\frac{1}{2}\kappa\rho + \Lambda, \quad (8)$$

$$3\frac{\dot{a}^2}{a^2} = \kappa\rho - 3\frac{k}{a^2} + \Lambda. \quad (9)$$

Equations (9) is sometimes written in terms of Ω s

$$1 = \Omega_m(t) + \Omega_k(t) + \Omega_\Lambda(t), \quad (10)$$

where $\Omega_m(t) = \frac{1}{3}\kappa\frac{\rho}{H^2}$, $\Omega_k(t) = -\frac{k}{H^2a^2}$, $\Omega_\Lambda(t) = \frac{1}{3}\frac{\Lambda}{H^2}$. This characterizes the evolution of spatially homogeneous FLRW models. Below it is shown that within a general class of the silent universes, the mean spatial curvature $\Omega_{\mathcal{R}}$ (in the FLRW limit $\Omega_{\mathcal{R}} \rightarrow \Omega_k$) will evolve from zero towards a negative non-negligible curvature.

2.1 The average spatial curvature

Within the silent universe, each worldline evolves independently, thus the volume average over a domain \mathcal{D} of a scalar function f is

$$\langle f \rangle_{\mathcal{D}} = \frac{\sum_i f_i V_i}{\sum_i V_i}, \quad (11)$$

where the volume of the domain \mathcal{D} is $V_{\mathcal{D}} = \sum_i V_i$, and the size of the domain is $r_{\mathcal{D}} = \left(\frac{3}{4\pi}V_{\mathcal{D}}\right)^{1/3}$. Averaging (6)

$$\frac{1}{6}\langle \mathcal{R} \rangle_{\mathcal{D}} = \frac{1}{3}\kappa\langle \rho \rangle_{\mathcal{D}} + \langle \Sigma^2 \rangle_{\mathcal{D}} - \frac{1}{9}\langle \Theta^2 \rangle_{\mathcal{D}} + \frac{1}{3}\Lambda \quad (12)$$

and introducing the domain Hubble parameter $H_{\mathcal{D}} = \frac{1}{3}\langle \Theta \rangle_{\mathcal{D}}$ we can rewrite the above equation (cf. eq. (10))

$$\Omega_{\mathcal{R}}^{\mathcal{D}} = 1 - \Omega_m^{\mathcal{D}} - \Omega_\Lambda^{\mathcal{D}} - \Omega_Q^{\mathcal{D}} \quad (13)$$

where

$$\begin{aligned}
\Omega_{\mathcal{R}}^{\mathcal{D}} &= -\frac{\langle \mathcal{R} \rangle_{\mathcal{D}}}{6H_{\mathcal{D}}^2}, \\
\Omega_m^{\mathcal{D}} &= \frac{8\pi G}{3H_{\mathcal{D}}^2} \langle \rho \rangle_{\mathcal{D}}, \\
\Omega_{\Lambda}^{\mathcal{D}} &= \frac{\Lambda}{3H_{\mathcal{D}}^2}, \\
\Omega_{\mathcal{Q}}^{\mathcal{D}} &= \frac{1}{H_{\mathcal{D}}^2} \left(\langle \Sigma^2 \rangle_{\mathcal{D}} + \frac{1}{9} \langle \Theta^2 \rangle_{\mathcal{D}} - H_{\mathcal{D}}^2 \right). \tag{14}
\end{aligned}$$

The above is often referred to as the *cosmic quartet* (Buchert, 2008), and $\Omega_{\mathcal{Q}}$ is the *kinematic backreaction* (Buchert, 2000) (to be precise, $\Omega_{\mathcal{Q}}$ is the dimensionless parameter of kinematic backreaction $\mathcal{Q}_{\mathcal{D}}$, which is defined as $\mathcal{Q}_{\mathcal{D}} = -6H_{\mathcal{D}}^2\Omega_{\mathcal{Q}} = \frac{2}{3}\langle \Theta^2 \rangle_{\mathcal{D}} - 6H_{\mathcal{D}}^2 - 2\langle \sigma^2 \rangle_{\mathcal{D}}$, where $2\sigma^2 = \sigma_{ab}\sigma^{ab} = 6\Sigma^2$).

The FLRW limit follows from eqs. (7)

$$\begin{aligned}
\Omega_{\mathcal{R}}^{\mathcal{D}} &\rightarrow \Omega_k = -\frac{k}{H^2 a^2}, \\
\Omega_m^{\mathcal{D}} &\rightarrow \Omega_m = \frac{8\pi G}{3H^2} \rho, \\
\Omega_{\Lambda}^{\mathcal{D}} &\rightarrow \Omega_{\Lambda} = \frac{1}{3H^2} \Lambda, \\
\Omega_{\mathcal{Q}}^{\mathcal{D}} &\rightarrow 0.
\end{aligned}$$

2.2 Setting up a Monte Carlo simulation of silent universes

The evolution of the universe is studied by performing a Monte Carlo simulation that is based on tracing the evolution of 2×10^6 worldlines. Each worldline is evolved by solving eqs. (1)–(4). This is done with the code *simsilun*¹ (Bolejko, 2017a). The initial conditions are set as perturbations around the Λ CDM background – it is assumed that the early universe is well approximated by the Λ CDM model. The Λ CDM model is defined by $\Omega_m = 0.308$, $\Omega_{\Lambda} = 0.692$, and $H_0 = 67.81 \text{ km s}^{-1} \text{ Mpc}^{-1}$ (Planck Collaboration et al., 2016). The initial instant is set to be an instant, which corresponds to $z_i = 200$ in the Λ CDM. This is to ensure smallness of initial perturbations, and to minimize the effect of pressure, which for $z < 200$ is below a percent level.

The initial density perturbation δ_i , for each worldline, is drawn from a Gaussian distribution with a standard deviation $\sigma_i = 0.0094$. This, ensures that the present-day standard deviation of the density contrast evaluated within spheres of radius $8h^{-1} \text{ Mpc}$ (which is a standard definition of the cosmological parameter σ_8) is $\sigma_8 = 0.82$ (Planck Collaboration et al., 2016).

¹<https://bitbucket.org/bolejko/simsilun>

Since the Monte Carlo simulation considered here, consists of 2×10^6 worldlines, thus 2×10^6 initial density contrasts δ_i are generated. These are then used to set up the initial conditions for ρ_i , Θ_i , Σ_i , and \mathcal{W}_i that are needed to solve eqs. (1)–(4). The initial conditions are evaluated based on the initial δ_i (Bolejko, 2017a).

$$\begin{aligned}
\rho_i &= \rho_{\Lambda\text{CDM}} + \Delta\rho = \rho_{\Lambda\text{CDM}}(1 + \delta_i), \\
\Theta_i &= \Theta_{\Lambda\text{CDM}} + \Delta\Theta = \Theta_{\Lambda\text{CDM}}\left(1 - \frac{1}{3}\delta_i\right), \\
\Sigma_i &= -\frac{1}{3}\Delta\Theta, \\
\mathcal{W}_i &= -\frac{1}{6}\Delta\rho,
\end{aligned} \tag{15}$$

where $8\pi G\rho_{\Lambda\text{CDM}} = \Omega_m 3H_0^2(1+z_i)^3$, and the value of the cosmological constant is $\Lambda = \Omega_\Lambda 3H_0^2$.

In addition, the volume around each worldline is calculated using eq. (5). The initial volume V_i follows from $V_i = M_i/\rho_i$, where it is assumed that each worldline has the same mass of $M_i = 1.6 \times 10^{14}M_\odot$. This value has been chosen for two reasons: 1) it is a mass of a small cluster or a small void, and 2) with this initial condition, the present day radius of an average cell (i.e. volume around each worldline) is $8h^{-1}$ Mpc. Thus, the total mass and the present-day size of a simulated universe are of order $10^{20}M_\odot$ and 10^9 pc, respectively.

3 Emergence of spatial curvature

The evolution of each worldline, within the studied Monte Carlo simulation, is evaluated from eqs. (1)–(4) using the code *simsilun* (Bolejko, 2017a). This allows for evaluating such quantities as density, expansion rate, and shear, from which using (6) the spatial curvature can be estimated. Using eq. (5) the evolution of the volume is evaluated, and then using eq. (11) the volume averages of these quantities are calculated. The resulted average density $\langle\rho\rangle_{\mathcal{D}}$, expansion rate $H_{\mathcal{D}}$, and spatial curvature $\Omega_{\mathcal{R}}^{\mathcal{D}}$ are presented in Fig. 1. These averages are evaluated by taking random domains of radius $r_{\mathcal{D}}$. For small values of $r_{\mathcal{D}}$, the density distribution is highly asymmetric with a long tail towards highly dense regions, which is a feature of a log-normal distribution observed in the galaxy surveys (Lahav & Suto, 2004). At $r_{\mathcal{D}} = 8h^{-1}$ Mpc ≈ 11.8 Mpc, the standard deviation of the density field is $\sigma_8 = 0.82$.

The most striking feature is that the mean does not coincide with the ΛCDM model. For $r_{\mathcal{D}} > 100$ Mpc, where the cosmic variance is negligible, the means are: $\langle\rho\rangle = 0.811\rho_{\Lambda\text{CDM}}$, $\langle H\rangle = 1.065H_0$, and $\Omega_{\mathcal{R}} = 0.153$. The reason why these means are not consistent with the ΛCDM model is presented in Fig. 2. Figure 2 shows the evolution of volume of the simulated universe (i.e. the volume occupied by 2×10^6 worldlines that constitute the Monte Carlo simulation). As seen the volume is larger than in the ΛCDM model (the volume of the ΛCDM model was calculated using the same setup, i.e. 2×10^6 worldlines but with $\delta_i = 0$, and it has been checked that the evolution indeed follows eqs. (8) and (9) with (7)). Since the mass is conserved and volume is larger, thus the average density is lower compared to the

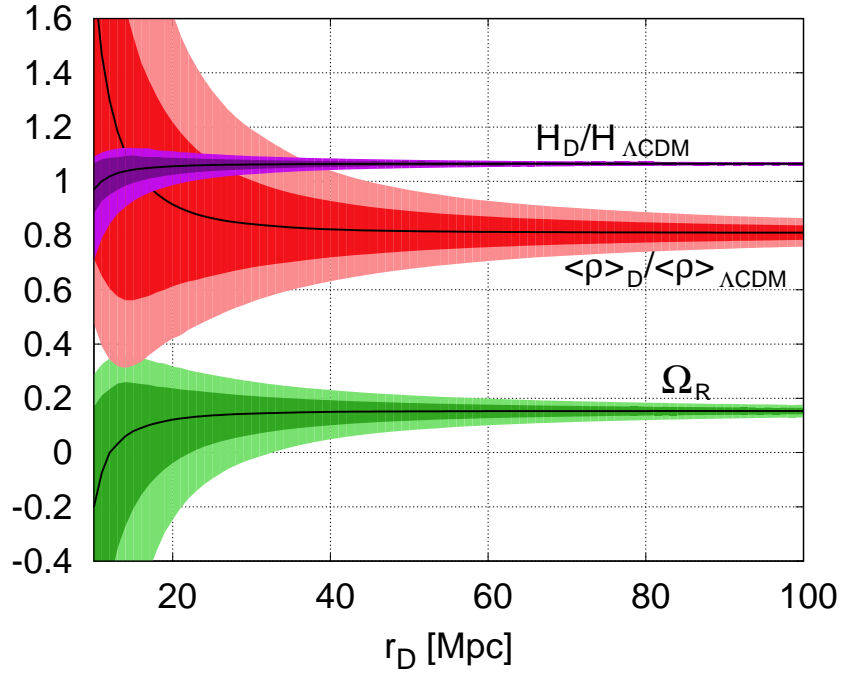


Figure 1: Volume averages at the present instant. Darker colors present the 68% scatter (i.e. 68% of values of averaging over random domains of size r_D fall within this interval) and lighter colors present 95% (i.e. 95% of values of averaging over random domains of size r_D fall within this interval). Beyond 100 Mpc the cosmic variance is negligible.

Λ CDM model. Another important feature presented in Fig. 2 is that the underdense regions, defined as regions with $\rho < 0.75\rho_{\Lambda\text{CDM}}$, occupy at the present instant approximately 80% of the total volume.

This phenomenon is of a nonlinear origin. As long as the perturbations are small and within the linear regime, their contribution to ρ and Θ is negligibly small and as seen from eqs. (1) and (2) all regions in the universe evolve in the same way. Once the evolution becomes nonlinear, both shear Σ^2 and density ρ , efficiently slow down the expansion rate of the overdense regions. Consequently they expand more slowly than the underdense regions. Subsequently, as follows from eq. (5), underdense regions occupy more volume than overdense regions, which is depicted in Fig. 2.

The phenomenon of breaking the symmetry between the evolution of the underdense and overdense regions leads to emerging negative spatial curvature of the universe. Tiny initial density perturbations, as follows from eq. (6), are also associated with curvature perturbations (negative for underdense and positive for overdense regions). In the course of evolution these tiny initial perturbations grow. The growth of the spatial curvature is also present in the FLRW model. As seen from eq. (10), $\Omega_k = -k/\dot{a}^2$. So if initially $k \neq 0$ then Ω_k is also non-zero and evolve as \dot{a}^{-2} . As long as the growth is linear the global average of the spatial curvature is zero – negative contribution from underdense regions is compensated by positive curvature of overdense regions. However, once the symmetry of evolution is broken by nonlinear evolution, the mean spatial curvature deviates from zero. This process is depicted in Fig. 3, which shows the relation between the present-day density variance measured with the parameter σ_8 and the present-day value of $\Omega_{\mathcal{R}}$. As described above, apart from the mass M_i (which is kept constant and the same for all worldlines), the only free parameter is the variance of the initial density field σ_i . The higher the initial variance σ_i , the larger the amplitude of initial perturbations, which eventually leads to a larger variance of the present-day density field (measured by σ_8). The larger the amplitude of initial perturbations, the quicker the evolution becomes nonlinear. Consequently the larger σ_i and σ_8 , the larger the present-day spatial curvature $\Omega_{\mathcal{R}}$. On the other hand, if the initial variance σ_i is very small (and so σ_8) the evolution of structures stays within the linear regime and does not enter the nonlinear stage. Subsequently, as seen in Fig. 3, for $\sigma_8 < 0.1$ the universe is still within the linear regime and stays spatially flat, confirming that the emergence of the spatial curvature is a feature of nonlinear evolution.

The evolution of the spatial curvature $\Omega_{\mathcal{R}}$ and other cosmic constituents, as defined by eqs. (14), is presented in Fig. 4. At the initial stages the system is dominated by matter but with time, the cosmological constant starts to dominate. In addition, when the evolution enters the nonlinear stage, the spatial curvature emerges, but then around 10 Gyr later it starts to decrease, which is related to the accelerated expansion caused by the cosmological constant. As above, this can be easily understood using the FLRW analogy; in the FLRW regime $\Omega_k \sim \dot{a}^{-2}$, so when the evolution start to accelerate, \dot{a} starts to increase and consequently Ω_k decreases. This is also known as the cosmological “no-hair” conjecture, which states that the dark energy dominated universe asymptotically approaches a homogeneous and isotropic de Sitter state (Pacher & Stein-Schabes, 1991), and as a results both $\Omega_{\mathcal{R}}$ and $\Omega_{\mathcal{Q}}$ after initial increase, asymptotically approach zero.

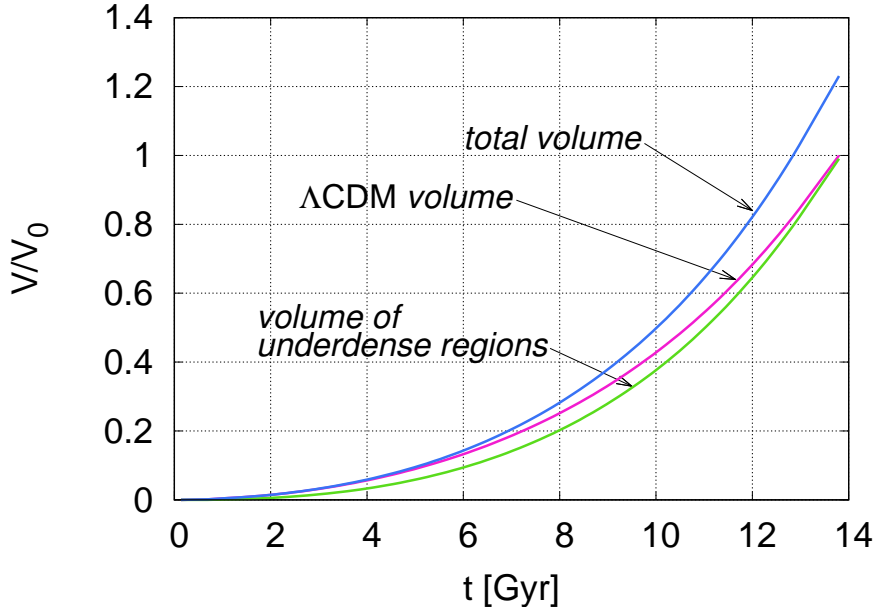


Figure 2: Evolution of the volume normilaised by the present day volume of the Λ CDM model V_0 : the total volume of the simulated Styrofoam universe (blue), the Λ CDM model (magenta), the volume of the regions with $\rho < 0.75\rho_{\Lambda CDM}$ (green).

4 Conclusions

This paper examined the emergence of the negative spatial curvature within a general class of silent universes. The analysis was based on the Monte Carlo simulation of 2×10^6 silent universes with the total mass of $3.2 \times 10^{20} M_{\odot}$. The initial conditions were set as perturbations around the Λ CDM model at the instant corresponding to $z = 200$. The analysis showed that once the evolution becomes nonlinear, the symmetry between the evolution of underdense and overdense regions is broken, and underdense regions start to occupy most of the volume of the Universe, reaching 80% at the present instant (Fig. 2). In the linear regime, the spatial curvature averages to 0 (see Fig. 3) but once the evolution is nonlinear the mean evolution deviates from 0 and evolves towards $\Omega_{\mathcal{R}}^D = 0.15$ at the present instant (see Fig. 4).

Another important results is that the current expansion rate is $\langle H \rangle_{\mathcal{D}} = 72.2 \text{ km s}^{-1} \text{ Mpc}^{-1}$, which is by 6% higher compared to the Λ CDM model of the early universe (see Fig. 1). This difference is a natural consequence of the universe dominated by voids, and could be an obvious solution to the widely debated discrepancy between the Hubble constant inferred from low-redshift observations $H_0 = 73.24 \pm 1.74 \text{ km s}^{-1} \text{ Mpc}^{-1}$ (Riess et al., 2016) and the one derived from the high-redshift data (CMB) $H_0 = 67.81 \pm 0.92 \text{ km s}^{-1} \text{ Mpc}^{-1}$ (Planck Collaboration et al., 2016).

The model discussed here, although quite general, has some limitations. The silent universes do not have pressure waves or gradients. As a result each worldline evolves indepen-

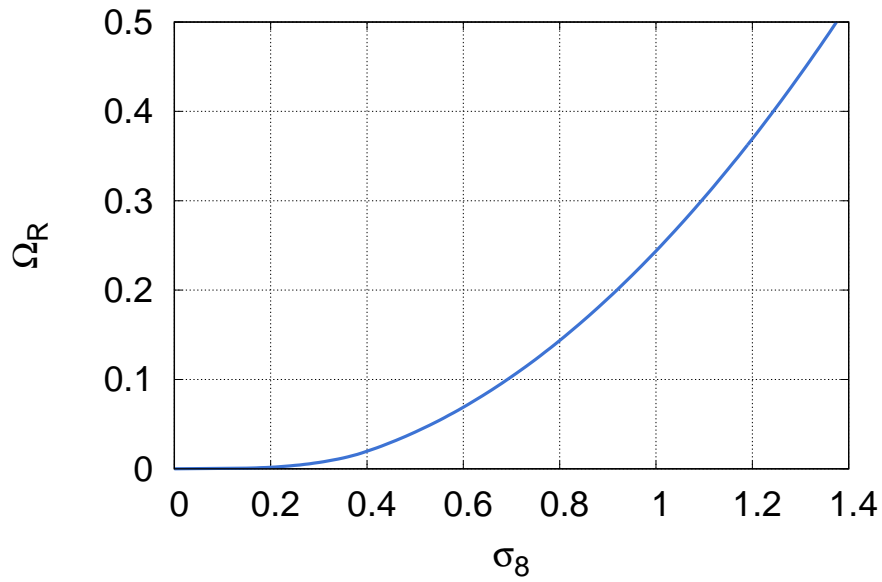


Figure 3: The role of nonlinear effects. The linear regime corresponds to small variance of the density field ($\sigma_8 < 0.1$) and at these scales the spatial curvature averaged over a domain of volume $V = (2150 \text{ Mpc})^3$ vanishes. With the increase of inhomogeneity, the system enters the nonlinear evolution quicker, leading also to higher values of the density variance, and resulting with large values of the global mean spatial curvature.

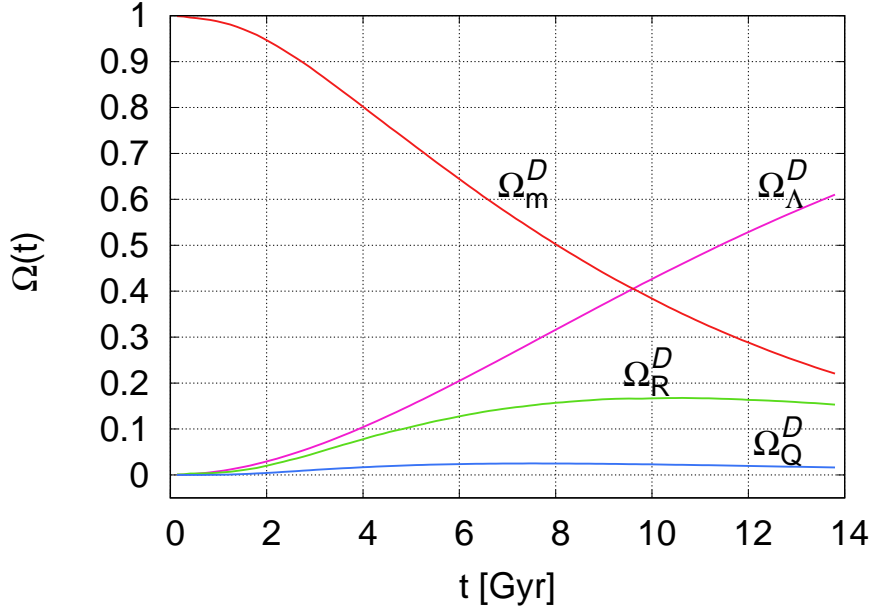


Figure 4: Cosmic quartet and its evolution (cf. eqs. (14)), with averages evaluated over a domain of mass $M = 3.2 \times 10^{20} M_\odot$. In the Λ CDM model, the present day values are $\Omega_m = 0.308$, $\Omega_\Lambda = 0.692$, and $\Omega_k = 0$ (in the FLRW limit $\Omega_R \rightarrow \Omega_k$ and $\Omega_Q = 0$).

dently. At scales below 2 Mpc where particle fluxes, multiple eigenvalues of the shear field, and rotation are important, the model loses its accuracy (Ellis & Tsagas, 2002). There are some indications that the small scales effects (< 1 Mpc) such as virialization (Roukema et al., 2013; Roukema, 2017) and the environmental dependent clock rates (Wiltshire, 2009) may enhance the discussed effects, but it seems that the fully relativistic modeling of these scales will only be achieved with numerical relativity (Bentivegna & Bruni, 2016; Mertens et al., 2016; Macpherson et al., 2017).

Therefore, the phenomenon of emerging curvature, presented here, should be considered as a theoretical speculation, and more work is needed to established the full magnitude to this phenomenon. What is encouraging, though, is that this phenomenon follows naturally from the nonlinear cosmic dynamics, and has a potential to explain some observational tensions such as a conflict between the low-redshift and high-redshift measurements of H_0 . It is also worth pointing out that the phenomenon of emerging curvature will soon be directly testable with observational data. As shown by Räsänen et al. (2015), using the data from surveys such as Euclid, and DES and LSST, we will be able to construct a Gpc-scale ‘cosmic triangle’ (with sides: observer-lens, observer-source, lens-source) and directly measure the curvature of the low-redshift universe ($z < 1$). By comparing low-redshift spatial curvature with the constraints obtained from high-redshift data (CMB), we will be able to test if the low-redshift and high-redshift constraints are different, which would empirically prove the phenomenon of the emerging spatial curvature. Such a procedure, has been presented in Fig. 5. Applying the

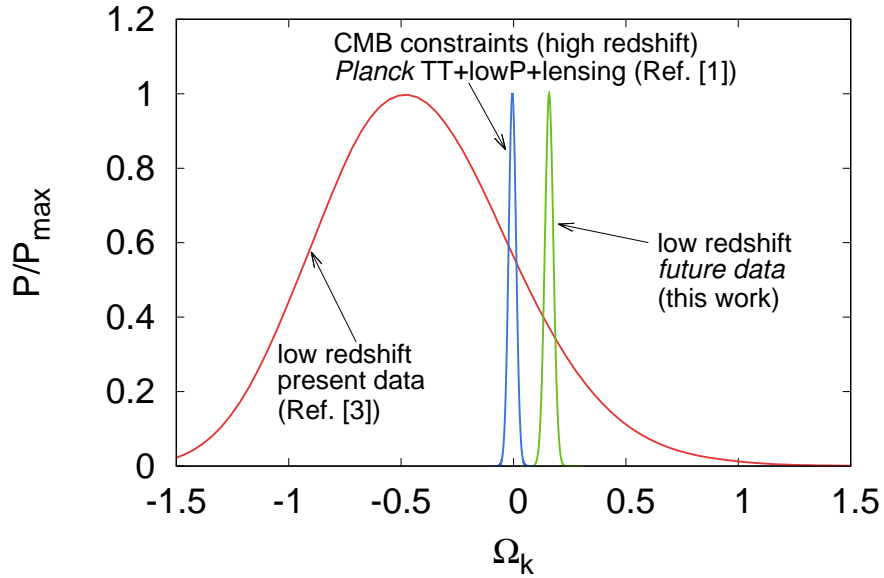


Figure 5: Constraints and predictions on the spatial curvature. The high redshift constraints (from CMB) are compared with the low-redshift constraints (based on the method described by Räsänen et al. (2015)). The current data are based on the Supplemental Material of Räsänen et al. (2015) and the future predictions are based on $2 \cdot 10^4$ simulated data (10^4 supernova data and 10^4 lensing data). In near future (5–7 years) we will be able to directly measure the curvature of the low-redshift universe and compare it to the spatial flatness of the high-redshift universe.

procedure discussed and presented by Räsänen et al. (2015) to the Monte Carlo simulation discussed in Sec. 3, the expected constraints are $\Omega_k = 0.15_{-0.03}^{+0.04}$ (95% confidence level). These constraints are based on simulated 10^4 lensed galaxies (expected from Euclid survey) and 10^4 supernova (expected from DES and LSST surveys), and are presented in Fig. 5. For comparison, Fig. 5 also shows constraints from present low redshift-data (supernova and lensing data obtained from the Supplemental Material of Räsänen et al. (2015)) and high-redshift data (*Planck* TT+LowP+lensing). Thus, as seen from Fig. 5, in the next 5–7 years the phenomenon of emerging spatial curvature will be directly testable.

Acknowledgement

This work was supported by the Australian Research Council through the Future Fellowship FT140101270.

References

- Bentivegna E., Bruni M., 2016, *Phys. Rev. Lett.*, 116, 251302
- Bolejko K., 2017a, preprint ([arXiv:1708.09143](https://arxiv.org/abs/1708.09143))
- Bolejko K., 2017b, *J. Cosmol. Astropart. Phys.*, 06, 025
- Bruni M., Matarrese S., Pantano O., 1995, *Astroph. J.*, 445, 958
- Buchert T., 2000, *Gen. Rel. Grav.*, 32, 105
- Buchert T., 2008, *Gen. Rel. Grav.*, 40, 467
- Buchert T., Carfora M., 2008, *Classical and Quantum Gravity*, 25, 195001
- Ellis G. F. R., Stoeger W. R., 2009, *Mon. Not. R. Astron. Soc.*, 398, 1527
- Ellis G. F. R., Tsagas C. G., 2002, *Phys. Rev. D*, 66, 124015
- Guth A. H., 1981, *Phys. Rev. D*, 23, 347
- Lahav O., Suto Y., 2004, *Living Reviews in Relativity*, 7, 8
- Macpherson H. J., Lasky P. D., Price D. J., 2017, *Phys. Rev. D*, 95, 064028
- Mertens J. B., Giblin J. T., Starkman G. D., 2016, *Phys. Rev.*, D93, 124059
- Pacher T., Stein-Schabes J. A., 1991, *Annalen der Physik*, 503, 518
- Planck Collaboration et al., 2016, *Astron. Astroph.*, 594, A13
- Räsänen S., Bolejko K., Finoguenov A., 2015, *Phys. Rev. Lett.*, 115, 101301

Riess A. G., et al., 2016, *Astroph. J.*, 826, 56

Roukema B. F., 2017, preprint, ([arXiv:1706.06179](https://arxiv.org/abs/1706.06179))

Roukema B. F., Ostrowski J. J., Buchert T., 2013, *J. Cosmol. Astropart. Phys.*, 10, 043

Roy X., Buchert T., Carloni S., Obadia N., 2011, *Classical and Quantum Gravity*, 28, 165004

Wiltshire D. L., 2009, *Phys. Rev. D*, 80, 123512

van Elst H., Uggla C., Lesame W. M., Ellis G. F. R., Maartens R., 1997, *Classical and Quantum Gravity*, 14, 1151